Electronic structure of the iron-based superconductor LaOFeP

D. H. Lu[1], M. Yi[1], S.-K. Mo[1,2], A. S. Erickson[3], J. Analytis[3], J.-H. Chu[3], D. J. Singh[4], Z. Hussain[2], T. H. Geballe[3], I. R. Fisher[3] & Z.-X. Shen[1]

The recent discovery of superconductivity in the iron oxypnictide family of compounds[1–9] has generated intense interest. The layered crystal structure with transition-metal ions in planar square-lattice form and the discovery of spin-density-wave order near 130 K (refs 10, 11) seem to hint at a strong similarity with the copper oxide superconductors. An important current issue is the nature of the ground state of the parent compounds. Two distinct classes of theories, distinguished by the underlying band structure, have been put forward: a local-moment antiferromagnetic ground state in the strong-coupling approach[12–17], and an itinerant ground state in the weak-coupling approach[18–22]. The first approach stresses on-site correlations, proximity to a Mott-insulating state and, thus, the resemblance to the high-transition-temperature copper oxides, whereas the second approach emphasizes the itinerant-electron physics and the interplay between the competing ferromagnetic and antiferromagnetic fluctuations. The debate over the two approaches is partly due to the lack of conclusive experimental information on the electronic structures. Here we report angle-resolved photoemission spectroscopy (ARPES) of LaOFeP (superconducting transition temperature, $T_c = 5.9$ K), the first-reported iron-based superconductor[2]. Our results favour the itinerant ground state, albeit with band renormalization. In addition, our data reveal important differences between these and copper-based superconductors.

In Fig. 1 we compare the angle-integrated photoemission spectrum (AIPES) with the density of states obtained from the local-density-approximation (LDA) band structure calculations. It is important to note that the peak near the Fermi level (E_F) is as strong as the valence band peak, in sharp contrast with the typical valence band spectrum of copper oxide superconductors, as shown in the inset of Fig. 1a. The valence band spectrum of copper oxide superconductors is characterized by a weak feature near E_F on top of a broad valence band peak, consistent with the doped-Mott-insulator picture. This clear disparity between the iron-based superconductor and the copper oxide superconductors suggests that itinerant-electron physics rather than Mott physics is a more appropriate starting point for the iron-based superconductors, at least for LaOFeP. Our data also disagree with some recent AIPES data[23,24] obtained from polycrystalline samples that show only a very small peak near E_F on top of a large valence band peak, which is reminiscent of the valence band spectra of copper oxide superconductors. This difference may be due to the surface quality of polycrystalline samples, as is often the case for oxides[25]. On balance, our data do not support theoretical models assuming strongly antiferromagnetic ground states (at least not those currently being formulated, albeit for the LaOFeAs system[12–15]), as there is no evidence in our spectra for exchange splitting of the iron *d*-electron states, and agreement between our valence band spectrum and the density of states calculated using such models is poorer in comparison with the density of states calculated in the LDA assuming an itinerant ground state.

More detailed information can be obtained from angle-resolved data. To understand the seemingly complex multiband electronic structure, we superimpose the LDA band structures on top of our data (Fig. 2). A quantitative agreement can be found between the angel-resolved photoemission spectra and the calculated band dispersions after shifting the calculated bands up by 0.11 eV and then renormalizing by a factor of 2.2. Note that the values of the E_F shift and the band renormalization factor are chosen to obtain the best match of the two higher binding energy bands at the Γ point. Although the renormalized bands using this set of parameters fit the bands near Γ very well, the match near the X point and the M point is less perfect. This suggests that different bands may have slightly different renormalization effects. Nevertheless, the overall level of agreement between the experiments and the calculations is significant, as nearly all features in our data have corresponding bands in the calculations, indicating that the LDA with the assumption of an itinerant ground state captures the essence of the electronic structure of this system. This again suggests that the iron-based superconductors, or at least LaOFeP, are different from copper oxide superconductors. We also note that the measured dispersions show no similarity with the band structure calculations of LaOFeAs calculated assuming an antiferromagnetic ground state[12–15].

To extract more information from angle-resolved photoemission spectra, a simple analysis of momentum distribution curves is done for the high-symmetry cuts. A Fermi velocity (v_F) of 1.0 ± 0.2 eV Å (equivalent to $(1.5 \pm 0.3) \times 10^5$ m s^{-1}) is obtained for all three bands individually. For comparison, the values extracted from the LDA calculations, after taking into account the E_F shift, are 1.5 or 1.7, 1.4, and 2.4 or 3.5 eV Å for the Γ_1, Γ_2 and M bands, respectively. Note that two different numbers are given for both the Γ_1 band and the M band because each contains two nearly degenerate bands. This observation demonstrates that the renormalization effects are different for different bands, as anticipated above, indicating that correlation effects are appreciable and not isotropic. However, these v_F renormalization values as well as the total-bandwidth rescaling factor of 2.2 are comparable to those of Sr_2RuO_4, which is a correlated Fermi liquid and is reasonably well described by theories using itinerant band structure as the starting point[26]. The corresponding electron-band masses m^* extracted from our data are, in units of the free electron mass, 1.4 ± 0.3, 4.6 ± 0.5 and 1.3 ± 0.3 for the Γ_1, Γ_2 and M bands, respectively. We note that the magnetic susceptibility enhancement compared with the bare-band-structure density of

[1]Department of Physics, Department of Applied Physics and Stanford Synchrotron Radiation Laboratory, Stanford University, Stanford, California 94305, USA. [2]Advanced Light Source, Lawrence Berkeley National Laboratory, Berkeley, California 94720, USA. [3]Geballe Laboratory for Advanced Materials and Department of Applied Physics, Stanford University, Stanford, California 94305-4045, USA. [4]Materials Science and Technology Division, Oak Ridge National Laboratory, Oak Ridge, Tennessee 37831-6114, USA.

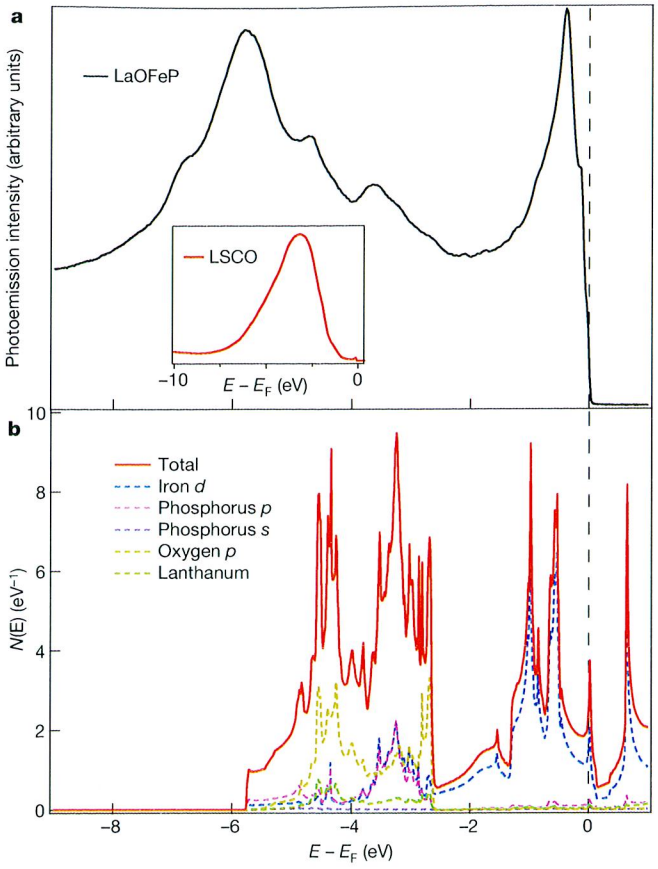

Figure 1 | Comparison between angle-integrated photoemission spectrum and calculated density of states. **a**, Valence band spectrum of LaOFeP taken with 42.5-eV photons using transmission mode (see Supplementary Information). It consists of a sharp, intense peak near the Fermi level that is separated from a number of broad peaks at higher binding energy. The inset shows the valence band of $La_{2-x}Sr_xCuO_4$ (LSCO), for comparison. **b**, LDA density of states and projections onto the linear-augmented-plane-wave spheres. According to the LDA calculations, the near-E_F states have dominant iron d-state character, whereas the peaks at higher binding energy are mixtures of oxygen p states and hybridized iron d and phosphorus p states. In comparison with the calculated density of states, the near-E_F peak has a narrower width than the calculated iron d states and is pushed closer to E_F, which is consistent with the band renormalization effect discussed in Fig. 2. The valence band peaks at higher binding energy, however, are shifted towards higher binding energy, resulting in slightly larger total valence band width.

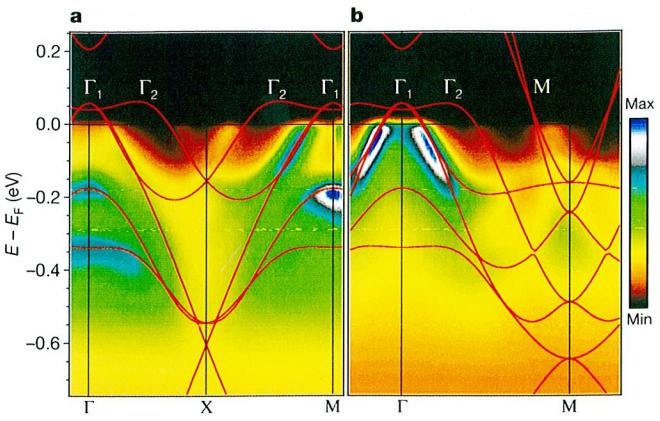

Figure 2 | Comparison between angle-resolved photoemission spectra and LDA band structures along two high-symmetry lines. ARPES data from LaOFeP (image plots) were recorded using 42.5-eV photons with an energy resolution of 16 meV and an angular resolution of 0.3°. For better comparison with experimental data, the LDA band structures using the experimental lattice parameters with relaxed internal atomic positions (see Supplementary Information) are shifted up by ~0.11 eV and then renormalized by a factor of 2.2 (red lines). **a**, Along the Γ–X direction, two bands crossing E_F can be clearly identified: one near the Γ point (Γ_1) and one near the X point (Γ_2). These two crossings are associated with two hole-like Fermi surface pockets centred at Γ. According to the LDA calculations, the inner pocket originates from iron d_{xz} and d_{yz} bands that are degenerate at Γ, and the splitting of these two bands close to Γ is too small to be resolved in our data. However, we do see evidence for the splitting at higher binding energy. The outer pocket is derived from the iron $d_{3z^2-r^2}$ states that hybridize with the phosphorus p orbitals and lanthanum orbitals. **b**, Along the Γ–M direction, three E_F crossings are observed in total. In addition to the two crossings associated with two hole pockets, a crossing near the M point can be observed, although the corresponding crossing in the second zone is too weak to be seen, owing to the matrix element effect. This crossing is related to the electron pocket centred at M. The LDA calculations also predict two bands crossing E_F around the M point, which cannot be clearly resolved in our data.

states is a factor of almost six[18], indicating either a lower-energy-scale renormalization or a strong Stoner renormalization. In this regard, we do not observe any apparent low-energy kink in the dispersion near 50 meV, which is a universal feature in copper oxide superconductors[27].

In Fig. 3 we display the energy distribution curves (EDCs) along the same high-symmetry cuts as shown in Fig. 2. Close inspection of these shows that there is no evident pseudogap within our experimental uncertainty in all three bands crossing the Fermi level, in contrast to the ubiquitous pseudogap observed in underdoped copper oxides. The absence of the pseudogap, therefore, marks an important difference between this new iron-based superconductor and copper oxide superconductors. This finding contradicts the recent report of a 20-meV pseudogap in LaOFeP from AIPES[28]. The difference can be attributed either to the polycrystalline samples used for that measurement having poor surface quality (previous work indicates potential problems associated with impurities[25]), or to distortion of the AIPES result by states away from the Fermi crossing (k_F). Angle-resolved photoemission spectroscopy of single-crystalline samples is much better suited to addressing the pseudogap issue by directly measuring the states near k_F. The same AIPES experiment[28] also indicated pseudogap effects with energy scales of 20 and 100 meV in polycrystalline $LaO_{1-x}F_xFeAs$ compounds, whereas another AIPES experiment[24] found a pseudogap of 15–20 meV in the same polycrystalline compounds. We cannot rule out the possibility of a pseudogap in arsenic-based compounds, which exhibit a spin-density-wave order in their parent compound LaOFeAs, as indicated in neutron scattering studies[10,11]. However, the similarly observed 20-meV pseudogap in polycrystalline samples of both LaOFeP and LaOFeAs (ref. 28) leads us to suggest a careful re-examination as soon as single crystals of the arsenic-based compounds become available.

Finally, we consider the Fermi surface topology (Fig. 4). Three sheets of Fermi surfaces are clearly observed: two hole pockets centred at Γ and one electron pocket centred at M. Keeping in mind the nearly degenerate Γ_1 and M bands, the observed Fermi surface topology is consistent with the five sheets of Fermi surfaces predicted in band structure calculations[29]. We note that the outer hole pocket Γ_2 originates from the hybridized iron $d_{3z^2-r^2}$ and phosphorus p states, which have strong k_z dispersion. The topology of this Fermi surface sheet is sensitive to the position of the phosphorus atoms, that is, the level of hybridization, and changes significantly upon doping. Calculating the Fermi surface volume enclosed by the three pockets yields respective electron counts of 1.94, 1.03 and 0.05 for the Γ_1, Γ_2 and M pockets. Taking into account the unresolved, nearly degenerate sheets under the Γ_1 and M pockets, a total electron count of 5.0 ± 0.1 is obtained, which is smaller than the expected value of 6. This is consistent with the need to shift E_F in order to produce the best fits of the dispersion in Fig. 2. It is too early to be certain how much of

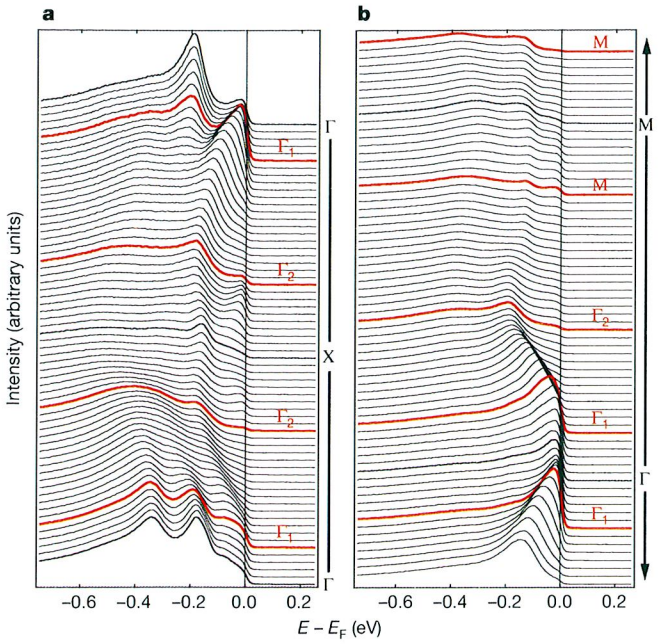

Figure 3 | Energy distribution curves along two high-symmetry lines. **a**, EDCs along the Γ–X direction. **b**, EDCs along the Γ–M direction. EDCs at k_F are plotted in red. The leading-edge midpoints of the red EDCs apparently reach E_F for all bands crossing E_F, indicating, within our experimental uncertainty, the absence of a pseudogap in this system.

this discrepancy is caused by a change in the surface doping, k_z dispersion or subtle surface-structure distortion, which can be significant for the Γ_2 band.

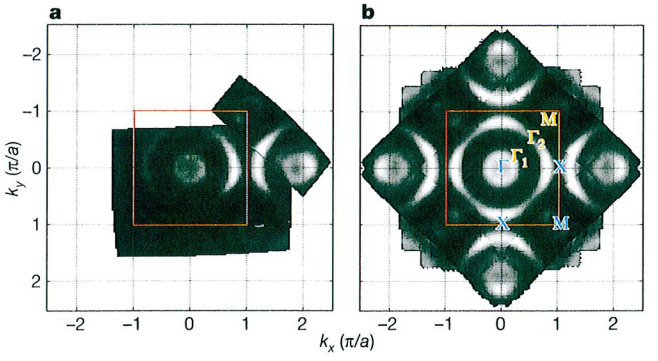

Figure 4 | Fermi surface maps of LaOFeP. **a**, Two sets of Fermi surface mapping (unsymmetrized raw data) are overlaid: the first set covers more than one Brillouin zone and the second set, taken mostly in the second Brillouin zone, yields a better view of the Fermi surface pocket at the M point, which is not well resolved in the first set owing to the polarization issue. The map is obtained by integrating the EDCs over an energy window of $E_F \pm 15$ meV. The red square highlights the boundary of the first Brillouin zone, where a is the in-plane lattice constant. **b**, Symmetrized Fermi surface map obtained by flipping and rotating the raw data shown in **a** along the high-symmetry lines to reflect the symmetry of the crystal structure. We use the Brillouin zone corresponding to the two-iron unit cell with the M point at (π, π), which is $(\pi, 0)$ in the large Brillouin zone for a simple iron square lattice. Three sheets of Fermi surfaces, labelled Γ_1, Γ_2 and M, are clearly observed. As discussed above (Fig. 2), Γ_1, the inner hole pocket observed in our data, should contain two nearly degenerate sheets, and the same is true for the electron pocket around M. Therefore, our data are consistent with the five sheets of Fermi surfaces predicted in band structure calculations[29]: two hole pockets around Γ, two electron pockets around M, and one highly three-dimensional hole pocket centred at Z.

Careful examination of the data in Fig. 3 reveals another possible discrepancy in band structure comparison, namely a very weak feature around −0.07 eV near Γ (Fig. 3a) that does not seem to have a corresponding band in LDA calculations. Further investigations are required to clarify its origin. Despite these disagreements, all the expected Fermi surface pieces are observed and are in good agreement with experiments in terms of the Brillouin zone locations and signs (hole versus electron). Furthermore, the measured main dispersions agree with the calculated band structures in great detail, as shown in Fig. 2. These observations make a strong case that the itinerant band structure captures the essence of the electronic structure of LaOFeP.

In summary, our ARPES data from LaOFeP suggest that the electronic structure of this material can be described using an itinerant band approach. In comparison with copper oxide superconductors, it has three important contrasting features: it has a much higher density of states near the Fermi level; it has multiple bands and Fermi surface sheets; and it shows no apparent evidence of the pseudogap effect.

Received 31 May; accepted 11 July 2008.

1. Day, C. New family of quaternary iron-based compounds superconducts at tens of kelvin. *Phys. Today* **61**, 11–12 (2008).
2. Kamihara, Y. *et al.* Iron-based layered superconductor: LaOFeP. *J. Am. Chem. Soc.* **128**, 10012–10013 (2006).
3. Kamihara, Y., Watanabe, T., Hirano, M. & Hosono, H. Iron-based layered superconductor $La[O_{1-x}F_x]FeAs$ ($x = 0.05–0.12$) with $T_c = 26$ K. *J. Am. Chem. Soc.* **130**, 3296–3297 (2008).
4. Takahashi, H. *et al.* Superconductivity at 43 K in an iron-based layered compound $LaO_{1-x}F_xFeAs$. *Nature* **453**, 376–378 (2008).
5. Chen, X. H. *et al.* Superconductivity at 43 K in $SmFeAsO_{1-x}F_x$. *Nature* **453**, 761–762 (2008).
6. Chen, G. F. *et al.* Superconductivity at 41 K and its competition with spin-density-wave instability in layered $CeO_{1-x}F_xFeAs$. *Phys. Rev. Lett.* **100**, 247002 (2008).
7. Ren, Z.-A. *et al.* Superconductivity at 52 K in iron-based F-doped layered quaternary compound $Pr[O_{1-x}F_x]FeAs$. Preprint at ⟨http://arxiv.org/abs/0803.4283⟩ (2008).
8. Ren, Z.-A. *et al.* Superconductivity at 55K in iron-based F-doped layered quaternary compound $Sm[O_{1-x}F_x]FeAs$. *Chin. Phys. Lett.* **25**, 2215–2216 (2008).
9. Wen, H.-H., Mu, G., Fang, L., Yang, H. & Zhu, X. Superconductivity at 25 K in hole doped $(La_{1-x}Sr_x)OFeAs$. *Europhys. Lett.* **82**, 17009 (2008).
10. de la Cruz, C. *et al.* Magnetic order close to superconductivity in the iron-based layered $LaO_{1-x}F_xFeAs$ systems. *Nature* **453**, 899–902 (2008).
11. Qiu, Y. *et al.* Neutron scattering study of the oxypnictide superconductor La(O,F)FeAs. Preprint at ⟨http://arxiv.org/abs/0805.1062⟩ (2008).
12. Cao, C., Hirschfeld, P. J. & Cheng, H. P. Proximity of antiferromagnetism and superconductivity in $LaO_{1-x}F_xFeAs$: effective Hamiltonian from ab initio studies. *Phys. Rev. B* **77**, 220506 (2008).
13. Haule, K., Shim, J. H. & Kotliar, G. Correlated electronic structure of $LaO_{1-x}F_xFeAs$. *Phys. Rev. Lett.* **100**, 226402 (2008).
14. Yin, Z. P. *et al.* Electron-hole symmetry and magnetic coupling in antiferromagnetic LaOFeAs. *Phys. Rev. Lett.* **101**, 047001 (2008).
15. Ma, F., Lu, Z.-Y. & Xiang, T. Antiferromagnetic superexchange interactions in LaOFeAs. Preprint at ⟨http://arxiv.org/abs/0804.3370⟩ (2008).
16. Fang, C., Yao, H., Tsai, W.-F., Hu, J. & Kivelson, S. Theory of electron nematic order in LaFeAsO. *Phys. Rev. B* **77**, 224509 (2008).
17. Xu, C., Mueller, M. & Sachdev, S. Ising and spin orders in iron-based superconductors. *Phys. Rev. B* **78**, 020501 (2008).
18. Singh, D. J. & Du, M.-H. Density functional study of $LaFeAsO_{1-x}F_x$: a low carrier density superconductor near itinerant magnetism. *Phys. Rev. Lett.* **100**, 237003 (2008).
19. Mazin, I. I., Singh, D. J., Johannes, M. D. & Du, M. H. Unconventional sign-reversing superconductivity in $LaFeAsO_{1-x}F_x$. *Phys. Rev. Lett.* (in the press); preprint at ⟨http://arxiv.org/abs/0803.2740⟩ (2008).
20. Zhang, H.-J., Xu, G., Dai, X. & Fang, Z. Enhanced orbital degeneracy in momentum space for LaOFeAs. Preprint at ⟨http://arxiv.org/abs/0803.4487⟩ (2008).
21. Raghu, S., Qi, X.-L., Liu, C.-X., Scalapino, D. & Zhang, S.-C. Minimal two-band model of the superconducting iron oxypnictides. *Phys. Rev. B* **77**, 220503 (2008).
22. Lee, P. A. & Wen, X.-G. Spin-triplet p-wave pairing in a 3-orbital model for FeAs superconductors. Preprint at ⟨http://arxiv.org/abs/0804.1739⟩ (2008).
23. Ou, H. W. *et al.* Angle integrated photoemission study of $SmO_{0.85}F_{0.15}FeAs$. *Chin. Phys. Lett.* **25**, 2225–2227 (2008).
24. Sato, T. *et al.* Superconducting gap and pseudogap in iron-based layered superconductor $La(O_{1-x}F_x)FeAs$. *J. Phys. Soc. Jpn* **77**, 063708 (2008).
25. Arko, A. *et al.* Large, dispersive photoelectron Fermi edge and the electronic structure of $YBa_2Cu_3O_{6.9}$ single crystals measured at 20 K. *Phys. Rev. B* **40**, 2268–2277 (1989).

26. Mackenzie, A. & Maeno, Y. The superconductivity of Sr_2RuO_4 and the physics of spin-triplet pairing. *Rev. Mod. Phys.* **75,** 657–712 (2003).
27. Lanzara, A. *et al.* Evidence for ubiquitous strong electron–phonon coupling in high-temperature superconductors. *Nature* **412,** 510–514 (2001).
28. Ishida, Y. *et al.* Evidence for pseudogap evolutions in high-T_c iron oxypnictides. Preprint at ⟨http://arxiv.org/abs/0805.2647⟩ (2008).
29. Lebegue, S. Electronic structure and properties of the Fermi surface of the superconductor LaOFeP. *Phys. Rev. B* **75,** 035110 (2007).

Supplementary Information is linked to the online version of the paper at www.nature.com/nature.

Acknowledgements We thank C. Cox, S. M. Kauzlarich and H. Hope for single-crystal X-ray diffraction measurements, and H. Yao, S. A. Kivelson, R. M. Martin, S. C. Zhang and X. L. Qi for discussions. ARPES experiments were performed at the Advanced Light Source, which is operated by the US Department of Energy Office of Basic Energy Science. Work at Stanford and Oak Ridge National Laboratory was supported by the Office of Basic Energy Science, Division of Materials Science and Engineering.

Author Information Reprints and permissions information is available at www.nature.com/reprints. Correspondence and requests for materials should be addressed to Z.-X.S. (zxshen@stanford.edu) or D.H.L. (dhlu@slac.stanford.edu).

This work was supported by the U.S. Department of Energy under Contract No. DE-AC02-05CH11231.

DISCLAIMER